Temperature dependence of luminescent spectra and dynamics in nanocrystalline Y2O3:Eu3+

Hongshang Peng, Hongwei Song, Baojiu Chen, Jiwei Wang, Shaozhe Lu et al.

Citation: J. Chem. Phys. **118**, 3277 (2003); doi: 10.1063/1.1538181
View online: http://dx.doi.org/10.1063/1.1538181
View Table of Contents: http://jcp.aip.org/resource/1/JCPSA6/v118/i7
Published by the American Institute of Physics.

Temperature dependence of luminescent spectra and dynamics in nanocrystalline Y_2O_3:Eu^{3+}

Hongshang Peng
Key Laboratory of Excited State Physics, Changchun Institute of Optics, Fine Machine, and Physics, Chinese Academy of Science, 140 People Street, Changchun 130022, People's Republic of China and College of Material, Jilin University, Changchun 130026, People's Republic of China

Hongwei Song,[a] Baojiu Chen, Jiwei Wang, Shaozhe Lu, Xianggui Kong, and Jiahua Zhang
Key Laboratory of Excited State Physics, Changchun Institute of Optics, Fine Machine, and Physics, Chinese Academy of Science, 140 People Street, Changchun 130022, People's Republic of China

(Received 12 February 2002; accepted 20 November 2002)

A temperature dependence for emission of Eu^{3+} in cubic nanocrystalline Y_2O_3:Eu^{3+} was studied in contrast with the polycrystalline powders. The emission intensity of Eu^{3+} decreased solely with elevated temperature under the excitation of a 580 nm light, while it had a maximum at a certain temperature under a 488 nm light. The experimental data were well fitted based on a theory considering both the thermal activated distribution of electrons among ^7F_J and the thermal quenching effect. The results indicated that the thermal quenching rate in nanocrystals (NCs) was faster than that in the polycrystals. The nonradiative decay rate, w_{NR}, the radiative transition rate, w_{0R}, and the luminescent quantum efficiency (QE) were obtained according to the temperature dependence of fluorescence lifetime. It can be concluded that w_{NR} and w_{0R} both increase in NCs, and that QE decreases. © *2003 American Institute of Physics.* [DOI: 10.1063/1.1538181]

I. INTRODUCTION

In 1994, Bhargava *et al.* reported that ZnS:Mn nanocrystals (NCs) were of much higher external luminescent quantum efficiency (QE) than the bulky ones.[1] Although this conclusion was seriously criticized later,[2] the studies on luminescent properties of doped NCs are attracting great interest now, because it is significant not only for applications but also for essential understanding of NCs. Among the nanosized luminescent materials, rare-earth-doped nanometer phosphors, which meet the demands of high-definition television, are intensively studied, since the resolution of image on a cathode ray tube display is related closely to the particle size of phosphors. As the main and unsurpassed red emitting materials in fluorescent lamps and projection television tubes, Y_2O_3:Eu^{3+} phosphors inevitably gather more attention.[3–6] Some work has been performed on the luminescent properties of Y_2O_3:Eu^{3+} NCs during the last few years.[7–10] However, the temperature-dependent luminescent properties in Y_2O_3:Eu^{3+} NCs were seldom studied, which is significant for understanding of the nonradiative and radiative transition processes. In this paper, we report the temperature dependence of emission spectra and the fluorescence lifetimes in Y_2O_3:Eu^{3+} NCs prepared by combustion synthesis, in contrast with those in the polycrystals (PCs).

II. EXPERIMENT

A. Sample preparation and characterization

The nanopowders of Y_2O_3:Eu^{3+} were prepared by combustion.[11] First, a solution was obtained by dissolving Eu_2O_3 (1% in the mol ratio) and Y_2O_3 in nitric acid. Then the glycine (Gly) was added subsequently. The mixed solution was gradually heated up in a beaker until it became sticky with the vaporizing of water. The system self-combusted for a few seconds as it reached a certain temperature. When the reaction finished, the Y_2O_3:Eu^{3+} NCs were obtained by collecting the resultant ashes. The size of NCs was controlled by the ratio of Gly/NO_3. The polycrystalline Y_2O_3:Eu^{3+} powders were prepared by high-temperature annealing at 1200 °C. The polycrystalline and nanocrystalline Y_2O_3 were cubic in symmetry, as confirmed by x-ray diffraction (XRD). Figure 1 shows the XRD spectrum of the cubic Y_2O_3:Eu^{3+} NCs. Using a sherrier formula, the size of Y_2O_3:Eu^{3+} NCs was determined to be ~4 nm based on the diffraction linewidth at an angle of 2θ=29.1. This was also confirmed by a survey of transition electronic microscopy micrograph.

B. Optical measurements

A continuous 488 nm light from an argon-ion laser was used as excitation. In the measurements, the samples were made into powder compact and put into a liquid nitrogen cycling system, in which the temperature varied form 77 to 670 K. The fluorescence was detected by a UV-Lab Raman Infinity (made by Jobin Yvon Company) with a resolution of 2 cm^{-1}.

A Rodamine 6 G dye laser pumped by a pulse

[a]Author to whom correspondence should be addressed. Electronic mail: songhongwei2000@sina.com.cn

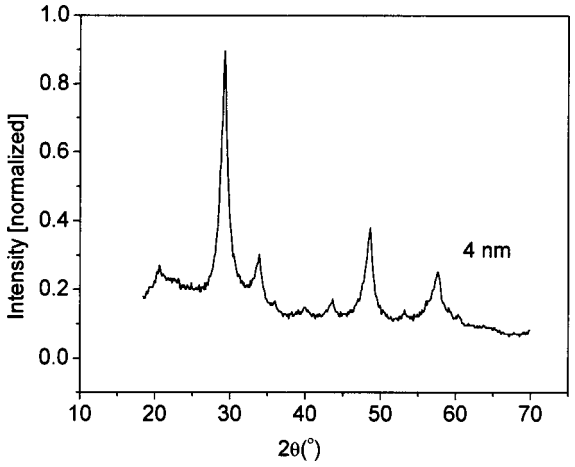

FIG. 1. X-ray diffraction pattern of cubic Y_2O_3:Eu^{3+} NCs (4 nm).

Nd^{3+}:yttrium–aluminum–garnet (YAG) laser (with a repetition frequency of 10 Hz and a duration of 10 ns) was used as resonant excitation source. In the measurements of fluorescence dynamics, a 355 nm light generated from the same Nd^{3+}:YAG laser combined with a third-harmonic generator was used as pumping. The powder samples were put into a liquid helium cycling system, where the temperature varied from 10 to 300 K. The emission spectra and decay dynamics were recorded by a spectrometer (Spex 1403) combined with a photomultiplier, a boxcar average, and a computer data acquisition.

III. RESULTS

A. Temperature dependence of the emission intensity of $^5D_0 \rightarrow {}^7F_2$ of Eu^{3+}

First, the emission spectra under the excitation of different lights were studied. Figures 2(a) and 2(b) show the emission spectra of Eu^{3+} in the NCs at various temperatures, respectively, under the excitation of the 580 and 488 nm lights. Under the 580 nm excitation, the emission intensity of $^5D_0 \rightarrow {}^7F_2$, which is dominant for the emissions of Eu^{3+}, remarkably decreases as the temperature increases. Under the 488 nm excitation, the emission intensity of $^5D_0 \rightarrow {}^7F_2$ is too weak to be detected at the range of 77–150 K. Above 200 K the emission intensity becomes detectable and grows rapidly as the temperature increases. It approaches a maximum at a certain temperature (~550 K), and then decreases as the temperature increases continuously. Similar results are also observed in the polycrystalline Y_2O_3:Eu^{3+} powders. The temperature dependencies of emission intensity of $^5D_0 \rightarrow {}^7F_2$ under the excitation of the 580 and 488 nm lights were drawn as Figs. 3(a) and 3(b), respectively. In Fig. 3 and the following test, the sample of PCs is labeled as A, and the 4 nm Y_2O_3:Eu^{3+} as B. In Fig. 3(a), it can be seen that the intensity in the NCs decreases faster than that in the polycrystalline ones as temperature increases. In Fig. 3(b), the intensity in NCs also decreases faster than that in the PCs above 550 K.

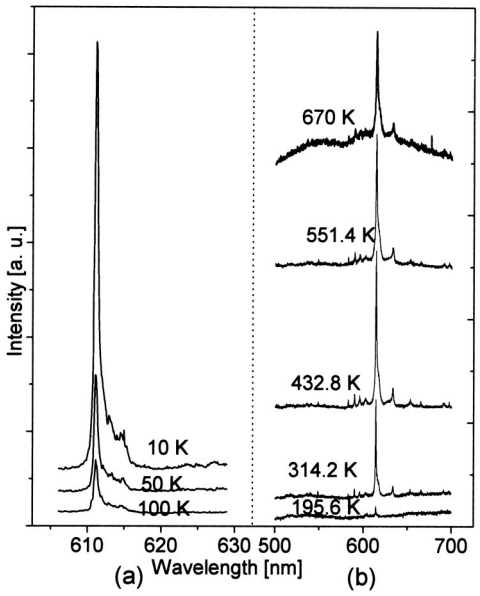

FIG. 2. Emission spectra of Eu^{3+} at various temperatures in the Y_2O_3:Eu^{3+} NCs under excitation of different lights (a) 580 nm; (b) 488 nm nm.

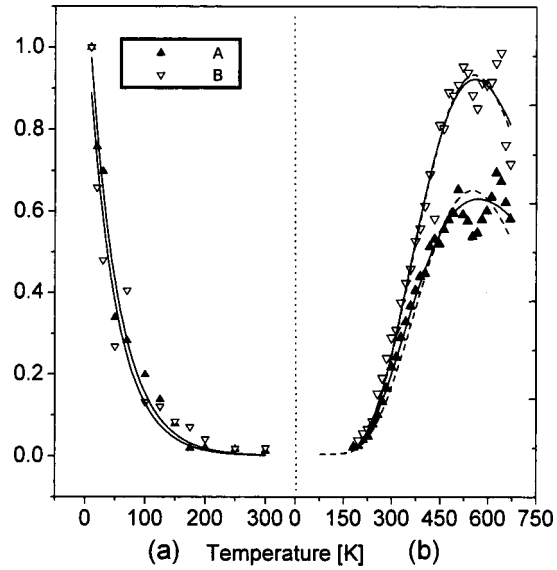

FIG. 3. Temperature-dependent emission intensity of Eu^{3+} under the excitation of different lights (a) 580 nm; (b) 488 nm. The dots are experimental data and the lines are fitting functions.

Under the 580 nm excitation (the 580 nm light is in resonance with the $^7F_0 \rightarrow {}^5D_0$ transition), there are two main factors leading the emission intensity of Eu^{3+} to decrease with the elevated temperature. One factor is the thermal activated distribution of electrons among ^7F_J. Since the ground state $^7F_0$ is close to the other states $^7F_1$ and $^7F_2$, some electrons on $^7F_0$ will be thermally excited into $^7F_1$ and $^7F_2$ as temperature increases, causing the electron population on $^7F_0$ and the resonant transition of $^7F_0 \rightarrow {}^5D_0$ to decrease. The other factor is the thermal quenching effect of luminescence, which is generally caused by nonradiative transition and energy transfer processes. According to steady-state luminescent dynamic equations, the emission intensity of $^5D_0 \rightarrow {}^7F_2$ can be approximately expressed as[12]

$$I(T) \propto \frac{I_C \sigma_0 n_0(T)}{1 + w_T / w_{0R}}, \tag{1}$$

where $n_0(T)$ is the population of $^7F_0$, σ_0 is the absorption cross section from $^7F_0 \rightarrow {}^5D_0$, I_C is the excitation intensity of the 580 nm light, w_T is the thermal quenching rate including the nonradiative transition rate of $^5D_0 \rightarrow {}^7F_6$ ($^7F_6$ is the nearest down level to $^5D_0$) and the energy transfer rate, w_{0R} is the radiative transition rate of $\Sigma {}^5D_0 \rightarrow {}^7F_J$ (J=0,1,2). Assuming that the electron population on $^7F_0$ is dominated by Boltzmann's distribution, i.e., $n_0(t) = n_0(0)/\Sigma_j g_J \exp(-\Delta E_{J0}/kT)$, and the thermal quenching rate is taken by the following empirical formula $w_T = w_T(0)\exp(T/T_c)$, where $n_0(0)$ is the population on $^7F_0$ at 0 K, $g_J = 2J+1$ is the energy level degeneracy of ^7F_J (J=0, 1, 2), ΔE_{J0} is the energy separation from ^7F_J to $^7F_0$ (J=1, 2), k is Boltzmann's constant, $w_T(0)$ is the thermal quenching rate at 0 K, T_c is a temperature constant. In this case, Eq. (1) can be written as

$$I(T) \approx \frac{\alpha}{\{[\Sigma_j g_J \exp(-\Delta E_{J0}/kT)(1 + \beta \exp(T/T_c)]\}}, \quad J = 0,1,2, \tag{2}$$

where $\alpha = I_C \sigma_0 n_0(0)$, $\beta = w_T(0)/w_{0R}$. By using Eq. (2), the emission intensity of Y_2O_3: Eu^{3+} was well fitted, which was drawn as lines in Fig. 3(a).

In fact, under the 488 nm excitation, the temperature dependence of the emission intensity of $^5D_0 \rightarrow {}^7F_2$ of Eu^{3+} is also dominated by the same two factors, the thermal activated distribution and the thermal quenching effect. As mentioned above, some of electrons can be thermally excited into $^7F_2$ as the temperature increases. The 488 nm photon is not in resonance with the $^7F_0 \rightarrow {}^5D_0$ transition, but in resonance with the $^7F_2 \rightarrow {}^5D_2$ transition considering the Stark splitting effect. The electron population on $^7F_2$ increases with the increasing temperature, causing the electrons optically excited to $^5D_2$ to increase and thus the emission intensity of $^5D_0 \rightarrow {}^7F_2$ to increase. On the other hand, the thermal quenching effect causes the emission intensity of $^5D_0 \rightarrow {}^7F_2$ to decrease. Considering these two factors, a maximum should appear in the temperature dependence of the emission intensity of Eu^{3+}. The thermal population of $^7F_2$ is dominated by $n_2(T) = n_0(0) g_2 \exp(-\Delta E_{20}/kT)/\Sigma_J g_J \exp(-\Delta E_{J0}/kT)$, thus the emission intensity under the 488 nm excitation can be approximately expressed as

$$I'(T) \approx \frac{\alpha' \exp(-\Delta E_{20}/kT)}{\{[\Sigma_J g_J \exp(-\Delta E_{J0}/kT)][1 + \beta \exp(T/T_c)]\}}, \quad J = 0,1,2, \tag{3}$$

where $\alpha' = I_c' \sigma_2 n_0(0) g_2$, σ_2 is the absorption cross section from $^7F_2 \rightarrow {}^5D_2$, I_c' is the excitation intensity of the 488 nm light. The temperature dependence of emission intensity of Eu^{3+} under the excitation of the 488 nm light was well fitted by using Eq. (3), which was shown as the solid lines in Fig. 3(b). For the PCs and NCs, the values of parameter T_c were determined to be 310 and 102 K, respectively. This means that the thermal quenching effect in the NCs is stronger than that in the PCs. We suggest that the stronger thermal quenching effect in NCs is related to surface effect. As known, a main characteristic for NCs is the increase of the surface/volume ratio. The increase of surface produces many surface defects and these defects generally act as nonradiative decay paths, causing the emission intensity as well as luminescent QE to decrease.

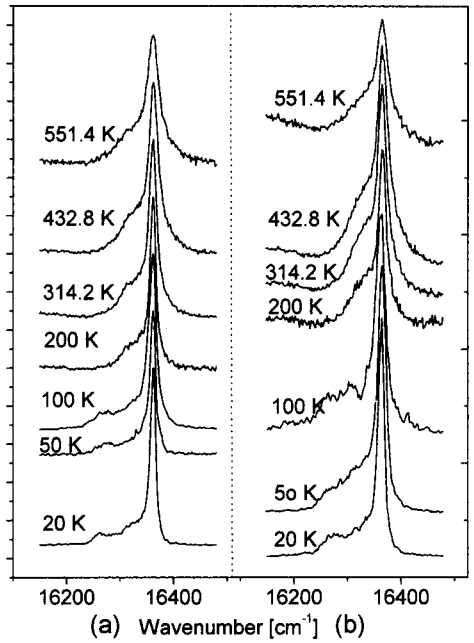

FIG. 4. Normalized emission spectra for the $^5D_0 \rightarrow {}^7F_2$ transition at various temperatures in different Y_2O_3:Eu^{3+} powders (a) polycrystalline; (b) 4 nm.

B. Temperature dependence of $^5D_0 \rightarrow {}^7F_2$ linewidths in Y_2O_3:Eu^{3+}

Figures 4(a) and 4(b) show, respectively, the $^5D_0 \rightarrow {}^7F_2$ linewidths of the polycrystalline and nanocrystalline Y_2O_3:Eu^{3+} at different temperatures. It is obvious that the linewidths are broadened as the temperature increases in the both crystals. The temperature dependence of the full linewidth of $^5D_0 \rightarrow {}^7F_2$ was drawn as Fig. 5. It is clear that the linewidths of $^5D_0 \rightarrow {}^7F_2$ in the two crystals both appropriately keep as constants below 70 K, and broaden with tem-

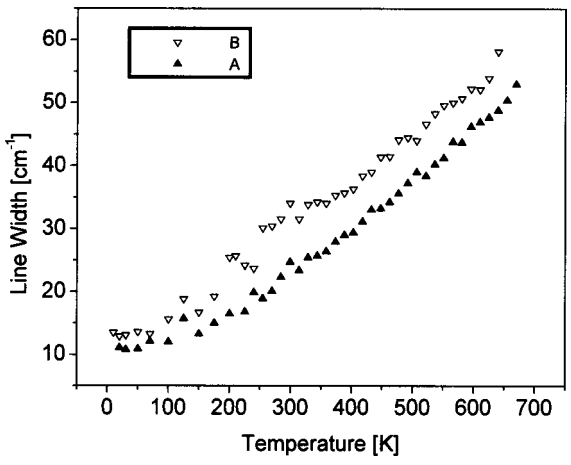

FIG. 5. Full linewidth of the $^5D_0 \rightarrow {}^7F_2$ transition vs temperature.

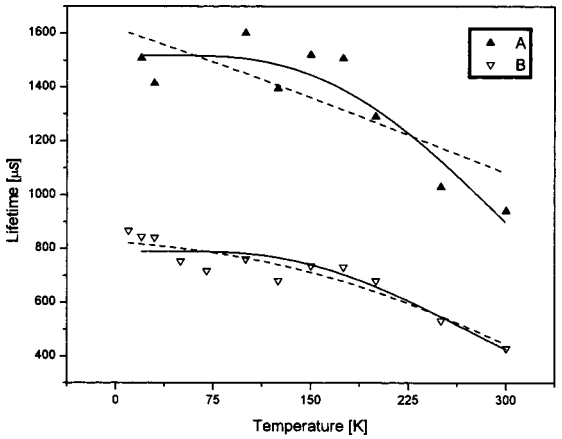

FIG. 6. Dependence of fluorescence lifetimes for the $^5D_0 \rightarrow {}^7F_2$ transition on temperature. The fluorescence decay curves were measured under the excitation of the 355 nm light with a delay of 100 μs. The solid lines are the fitting results by Eq. (6).

perature nearly following a linear behavior above 70 K. The linewidth of $^5D_0 \rightarrow {}^7F_2$ in the NCs is always broader than that in the PCs at any temperature. From 10 to 670 K, the linewidth increases several times. Generally, inhomogeneous linewidth varies only a little with temperature, while homogeneous linewidth strongly depends on temperature. By using the Debye model and assuming the dephasing processes as a two-phonon Raman process, the temperature dependence of homogeneous linewidth in bulky crystals has been well understood to follow a T^7 behavior when $T \ll \Theta_D$ (the Debye temperature), and a quadratic behavior when $T \gg \Theta_D$.[13] Meltzer and Hong studied the dephasing process in nanocrystalline Eu_2O_3 by persistent spectral hole burning and compared with that in the bulky one.[14] At low temperature (4–20 K) a T^α ($3.5 > \alpha > 3$) relationship was experimentally observed in nanocrystalline Eu_2O_3, which was well explained by the dephasing theory considering the confinement effect. In our experiments, the relationship between the full linewidth is contributed by several factors, including the homogeneous line broadening, the inhomogeneous line broadening, and the limitation of the apparatus. In Fig. 5, the full linewidth of $^5D_0 \rightarrow {}^7F_2$ in the NCs is larger than that in the PCs. One possible reason is that NCs have a size distribution, leading the linewidth to broaden. The other possible reason is the stronger electron–phonon interaction due to size effect. Hong *et al.* observed that the homogeneous linewidth for the $^7F_0 \rightarrow {}^5D_0$ transition of Y_2O_3:Eu^{3+} NCs increased in comparison to that of the bulky ones.[15]

C. Temperature dependence of $^5D_0 \rightarrow {}^7F_2$ fluorescence lifetimes

The fluorescence decay curves of $^5D_0 \rightarrow {}^7F_2$ at various temperatures were measured under the excitation of the 355 nm light, and the lifetimes were obtained by single-exponential fitting. The dependence of fluorescence lifetime on temperature was shown in Fig. 6. It is obvious that the fluorescence lifetimes of $^5D_0 \rightarrow {}^7F_2$ in the NCs are shorter than those in the PCs. In fact, the lifetime of $^5D_0$, τ is dominated by the radiative transition rate, w_{0R}, and the nonradiative decay rate, w_{NR}, which can be written as

$$\tau = \frac{1}{w_{0R} + w_{\mathrm{NR}}(T)}. \tag{4}$$

Generally, w_{NR} increases remarkably with elevated temperature, while w_{0R} has little change. The nonradiative decay of $^5D_0$ should include the nonradiative transition of $^5D_0 \rightarrow {}^7F_2$ and the energy transfer from $^5D_0$ to the other Eu^{3+} and/or the other impurity centers. Because the energy separation between $^5D_0$ and $^7F_6$ is as large as $\sim 12\,000\ \mathrm{cm}^{-1}$, the multiphonon nonradiative transition hardly happens. Thus, we assume that the nonradiative transition rate of $^5D_0 \rightarrow {}^7F_2$ in comparison with the energy transfer rate is negligible and the energy transfer is a multi-phonon process. During this process, the energy in $^5D_0$ state is transferred to quenching centers and several phonons are consequently released. According to the theory of multiphonon relaxation, the nonradiative decay rata of $^5D_0$ can be written as[16]

$$w_{\mathrm{NR}}(T) = w_{\mathrm{NR}}(0)(1 + \langle m \rangle)^{\Delta E/\hbar\omega} \tag{5}$$

with $w_{\mathrm{NR}}(0) = c \exp(-\alpha \Delta E)$, where c and α are constants dependent on host and almost independent of temperature, ΔE is the energy difference of the two states between which the multi-phonon relaxation happens, $\langle m \rangle = 1/[1 - \exp(-\hbar\omega/kT)]$ is phonon density, $\hbar\omega$ is phonon energy. Based on the Eqs. (4) and (5), the lifetime of $^5D_0$ as a function of temperature can be written as

$$\tau = \frac{1}{w_{0R} + w_{\mathrm{NR}}(0)[1 - \exp(-\hbar\omega/kT)]^{-\beta}}, \tag{6}$$

where $\beta = \Delta E/\hbar\omega$. The data in Fig. 6 were well fitted by using Eq. (6), as shown. In the fitting, we chose $\hbar\omega = 377\ \mathrm{cm}^{-1}$, which was determined by micro-Raman scattering spectra. (This energy is corresponding to the peak energy of one vibration mode in Y_2O_3: Eu^{3+}.) The parameters w_{0R}, $w_{\mathrm{NR}}(0)$ and β obtained by fitting were listed in Table I.

TABLE I. A list of parameters w_{0R}, $w_{\mathrm{NR}}(0)$ and β obtained by formula (6) in different Y_2O_3:Eu^{3+} powders.

Parameters	Sample A	Sample B
$w_{0R}(s^{-1})$	536	923
$w_{\mathrm{NR}}(0)(s^{-1})$	124	344
β	8.6	7.9

It should be noted that the temperature-dependent fluorescence lifetime has been fitted by assuming that nonradiative decay rate, w_{NR}, is equal to the thermal quenching rate, w_T. The fitting lines did not go well with the data points, which were shown as dash lines in Fig. 6. Also, we have fitted the temperature dependence of fluorescence intensity by assuming the thermal quenching as a multi-phonon process. The fluorescence intensity under the excitation of the 488 nm light was well fitted, which was drawn as dash lines in Fig. 3(b). However, the intensity under the excitation of the 580 nm light could not be well fitted. This was just the reason that we could not fit the temperature dependence of

the fluorescence quenching and that of the fluorescence lifetime with united formula of the nonradiative decay rate.

The fitting results listed in Table I indicate that w_{0R} and $w_{\mathrm{NR}}(0)$ in the NCs both increase in comparison with those in the PCs and $w_{\mathrm{NR}}(0)$ changes with particle size more rapidly than w_{0R} does. The electronic properties of nanometer particles contain two folds: (1) the quantum size effect, as a consequence of the reduction of quantum mechanical allowed states in a small particle, results in an increased band gap and an increased radiative transition rate and (2) the increase of the surface/volume ratio. The increase of nonradiative decay rate in Y_2O_3:Eu^{3+} may be attributed to the influence of surface defects, as mentioned above. Is the increase of radiative transition rate in Y_2O_3:Eu^{3+} caused by the electronic size effect? The answer is negative. In rare earth ions, the diameter of electronic wave function of *f* state is in the order of 10^{-1} nm, which is much smaller than the present particle size of Y_2O_3:Eu^{3+}, 4 nm. In this case, the quantum size effect does not work at all. We suggest that the increase of the radiative transition rate may be related to the degeneration of the crystal field around Eu^{3+} ions. Igarashi *et al.* reported the lattice distortion of the NCs was seven times larger than that of the micrometer particles.[17] The lattice distortion should decrease the lattice symmetry and strengthen the oscillator intensity. We consider that the lattice distortion in the present Y_2O_3:Eu^{3+} NCs is stronger than that in the PCs, which leads to the increase of the radiative transition rate. It should be pointed out that several groups reported that the $^5D_0$ lifetimes increased as the particle size decrease, which was attributed to the decrease of radiative transition rate with the decreasing particle size.[9,10,18] The different lifetimes may be caused by different sample preparation. Further work should be performed to compare the luminescent properties of Y_2O_3:Eu^{3+} NCs prepared by various methods.

In Ref. 18, Meltzer *et al.* reported that the radiative lifetime of the electronic transitions of an ion embedded in a medium could be described by the formula

$$\tau_R \sim \frac{1}{f(ED)} \frac{\lambda_0^2}{[\frac{1}{3}(n_{\mathrm{eff}}^2+2)]^2 n_{\mathrm{eff}}}, \tag{7}$$

with $n_{\mathrm{eff}}=xn_{Y_2O_3}+(1-x)n_{\mathrm{med}}$, where $f(ED)$ is the oscillator strength for the electric dipole transition, λ_0 is the wavelength in vacuum, n_{eff} is the effective refractive index, x is the ''filling factor'' showing what fraction of space is occupied by the Y_2O_3 nanocrystals, $n_{Y_2O_3}$ is the refractive index of Y_2O_3 and n_{med} is the refractive index of the media. According to the definition of n_{eff}, n_{eff} in NCs is smaller than that in PCs. After being modified by Eq. (7), it is clear to see that the increase of w_{0R} in the NCs is more prominent in comparison to that in the PCs.

As is well known, the luminescent QE can be written as $\eta=w_{0R}/[w_{0R}+w_{\mathrm{NR}}(T)]$. According to the fitting values determined by Eq. (6) and the QE formula, we calculated QE as a function of temperature, which was shown in Fig. 7. It is obvious that the QE of Eu^{3+} decreases as the temperature increases in the both crystals. Compared to the PCs the QE in the NCs becomes lower.

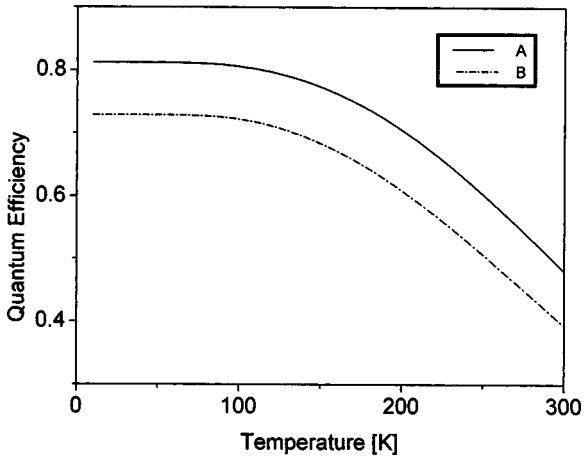

FIG. 7. Calculated QE of Eu^{3+} as a function of temperature in different sized Y_2O_3:Eu^{3+} powders.

IV. CONCLUSIONS

The temperature dependencies of fluorescence intensity, linewidth and lifetime for $^5D_0 \rightarrow {}^7F_2$ transition of Eu^{3+} in Y_2O_3:Eu^{3+} NCs were studied in contrast to the PCs. It was observed that the emission intensity of Eu^{3+} decreased solely with elevated temperature under the excitation of the 580 nm light, while it had a maximum at a certain temperature under the 488 nm light. The experimental data were well fitted according to the theory considering both the thermal activated distribution of electrons among ^7F_J and the thermal quenching effect. The fitting results indicate that the thermal quenching rate in the NCs is faster than that in the PCs. It is attributed to the influence of surface defects.

In Y_2O_3:Eu^{3+}, the full linewidth for the emission of $^5D_0 \rightarrow {}^7F_2$ increases linearly with temperature above 70 K, for both the NCs and PCs.

Some microscopic parameters such as w_{0R} and w_{NR} were determined based on the temperature dependence of fluorescence lifetime. The results indicate that in Y_2O_3:Eu^{3+} NCs, w_{0R} and w_{NR} both become larger than those in the PCs. The increase of w_{0R} in NCs is attributed to the lattice distortion, while the increase of w_{NR} is attributed to the influence of surface defects on nonradiative transition. Because w_{NR} varies more rapidly with particle size than w_{0R} does, the luminescent quantum efficiency of Eu^{3+} in NCs becomes lower.

ACKNOWLEDGMENT

This work was supported by the One Hundred Talents Project from the Chinese Academy of Science.

[1] R. N. Bhargava, D. Gallagher, X. Hong, and A. Nurmikko, Phys. Rev. Lett. **72**, 416 (1994).
[2] A. A. Bol and A. Meijerink, J. Lumin. **87–89**, 315 (2000).
[3] N. C. Chang, J. Appl. Phys. **34**, 3500 (1965).
[4] H. Forest and G. Ban, J. Electrochem. Soc. **116**, 474 (1969).
[5] B. M. Smets, Mater. Chem. Phys. **16**, 283 (1994).
[6] C. R. Ronda, J. Lumin. **72–74**, 49 (1997).

[7] H.-S. Yang, K. S. Hong, S. P. Feofilov, B. M. Tissue, R. S. Meltzer, and W. M. Dennis, J. Lumin. **83,84**, 139 (1999).
[8] A. Konrad, T. Fries, A. Gahn, and F. Kummer, J. Appl. Phys. **86**, 3129 (1999).
[9] D. K. Williams, H. Yuan, and B. M. Tissue, J. Lumin. **83,84**, 297 (1999).
[10] R. Schmechel, M. Kennedy, and H. von Seggern, J. Appl. Phys. **89**, 1679 (2001).
[11] T. Ye, G. Zhao, W. Zhang, and S. Xia, Mater. Res. Bull. **32**, 501 (1997).
[12] J. Wang, H. Song, X. Kong, and W. Xu, J. Appl. Phys. **91**, 9466 (202).
[13] H. Maier, B. Kharlamov, and D. Haarer, in *Investigation of Tunneling Dynamics by Optical Hole-Burning Spectroscopy*, edited by P. Esquinazi (Springer, Berlin, 1998), p. 321.
[14] R. S. Meltzer and K. S. Hong, Phys. Rev. B **61**, 3396 (2000).
[15] K. S. Jong, R. S. Meltzer, B. Bihari, D. K. Williams, and B. M. Tissue, J. Lumin. **76,77**, 234 (1998).
[16] B. Reisfeld and Y. Eckstein, J. Chem. Phys. **63**, 4001 (1975).
[17] T. Igarashi, M. Ihara, T. Kusunoki, K. Ohno, T. Isobe, and M. Senna, Appl. Phys. Lett. **76**, 1549 (2000).
[18] R. S. Meltzer, S. P. Feofilov, B. Tissue, and H. B. Yuan, Phys. Rev. B **60**, R14012 (1999).